JCI insight

RESEARCH ARTICLE

Two human patient mitochondrial pyruvate carrier mutations reveal distinct molecular mechanisms of dysfunction

Lalita Oonthonpan,[1] Adam J. Rauckhorst,[1] Lawrence R. Gray,[1] Audrey C. Boutron,[2] and Eric B. Taylor[1,3,4,5,6]

[1]Department of Biochemistry, Carver College of Medicine, University of Iowa, Iowa City, Iowa, USA. [2]Biochemistry Department, CHU Bicetre, Hôpitaux Paris-Sud, Assistance Publique – Hôpitaux de Paris, Paris, France. [3]Fraternal Order of Eagles Diabetes Research Center (FOEDRC), [4]Abboud Cardiovascular Research Center, [5]Holden Comprehensive Cancer Center, and [6]Pappajohn Biomedical Institute, Carver College of Medicine, University of Iowa, Iowa City, Iowa, USA.

The mitochondrial pyruvate carrier (MPC) occupies a central metabolic node by transporting cytosolic pyruvate into the mitochondrial matrix and linking glycolysis with mitochondrial metabolism. Two reported human *MPC1* mutations cause developmental abnormalities, neurological problems, metabolic deficits, and for one patient, early death. We aimed to understand biochemical mechanisms by which the human patient C289T and T236A *MPC1* alleles disrupt MPC function. *MPC1* C289T encodes 2 protein variants, a misspliced, truncation mutant (A58G) and a full-length point mutant (R97W). *MPC1* T236A encodes a full-length point mutant (L79H). Using human patient fibroblasts and complementation of CRISPR-deleted, *MPC1*-null mouse C2C12 cells, we investigated how *MPC1* mutations cause MPC deficiency. Truncated MPC1 A58G protein was intrinsically unstable and failed to form MPC complexes. The MPC1 R97W protein was less stable but, when overexpressed, formed complexes with MPC2 that retained pyruvate transport activity. Conversely, MPC1 L79H protein formed stable complexes with MPC2, but these complexes failed to transport pyruvate. These findings inform MPC structure-function relationships and delineate 3 distinct biochemical pathologies resulting from 2 human patient *MPC1* mutations. They also illustrate an efficient gene pass-through system for mechanistically investigating human inborn errors in pyruvate metabolism.

Introduction

Pyruvate is a critical metabolite linking fundamental metabolic processes across the cytosol and mitochondria. Cytosolic reduction of pyruvate to lactate maintains NAD+ pools required for glycolysis (1, 2). The reversible transamination of pyruvate to alanine in both the cytosol and mitochondria coordinates carbohydrate and amino acid metabolism (3). Mitochondrial pyruvate may be converted to acetyl-CoA for tricarboxylic acid (TCA) cycle oxidation and cellular respiration (4). Furthermore, mitochondrial pyruvate may be utilized anaplerotically, by conversion to oxaloacetate, to replenish the TCA cycle when intermediates are withdrawn for biosynthesis (5). The centrality of pyruvate to these fundamental processes illustrates the impact of pyruvate metabolism on cellular function.

Further underscoring the importance of pyruvate metabolism, mutations in genes regulating pyruvate metabolism lead to devastating multi-system deficits (6). Clinical presentations of inborn errors in pyruvate metabolism usually involve elevated blood pyruvate, lactate, and alanine (6). Neurological abnormalities are often observed, but the severity and biochemical manifestations depend on the nature of the mutation and unique genetics and physiology of the patient. Indeed, the transporter that conducts pyruvate across the mitochondrial inner membrane was identified in part by localizing mutations underlying pyruvate metabolism deficits in human patients (7, 8).

In flies, rodents, and humans, the mitochondrial pyruvate carrier (MPC) is a hetero-oligomer consisting of 2 obligate protein subunits, MPC1 and MPC2, encoded by the *MPC1* and *MPC2* genes (7, 9). The loss of either subunit leads to loss of the other and the MPC complex, and recent findings indicate an MPC1-MPC2 heterodimer functions as the active MPC complex (7, 9, 10). Disruption of MPC activity

Conflict of interest: EBT has received research grant funding administered through the University of Iowa from Cirius Therapeutics.

Submitted: November 12, 2018
Accepted: May 24, 2019
Published: July 11, 2019.

Reference information: *JCI Insight*. 2019;4(13):e126132. https://doi.org/10.1172/jci.insight.126132.

by genetic or chemical mechanisms ablates direct mitochondrial pyruvate uptake, thereby eliminating a central node in cellular metabolism.

Multiple lines of evidence show the MPC plays key roles in health and disease. Disruption of the liver MPC lowers blood glucose during diabetes (11, 12), and attenuates non-alcoholic steatohepatitis (NASH; refs. 13, 14). Conversely, decreased MPC expression and activity increases stemness in some cancers (15–19). The MPC appears to play an especially critical role during development. Whole-body genetic MPC disruption is embryonic lethal in mice (20, 21). In humans, 2 reported *MPC1* mutations cause developmental abnormalities, neurological problems, metabolic deficits marked by high blood pyruvate and lactate, and, in the case of one patient, death early in childhood (7, 8).

The C289T *MPC1* allele was previously reported to produce 2 transcripts (7). One is misspliced and predicted to generate a frame-shifted, truncated protein (A58GfsX2; herein referred to as A58G). The other is predicted to generate a full-length protein with a conserved arginine changed to tryptophan (R97W). The T236A *MPC1* allele is predicted to generate a full-length protein with a conserved leucine changed to histidine (L79H). How these mutations affect MPC protein content, complex stability, and function has not been delineated.

Here, we aimed to understand biochemical mechanisms by which the human patient *MPC1* C289T and T236A alleles disrupt MPC function. We utilized human patient fibroblasts and developed a novel, to our knowledge, heterologous gene complementation system with the highly metabolically active mouse C2C12 myoblast cell line. C2C12 cells were treated with CRISPR/Cas9 to generate *Mpc1*-null (*ΔMpc1*) lines. *ΔMpc1* C2C12 cells were then complemented with both artificially truncated and human patient *MPC1* alleles. Complemented cells were tested for changes in mitochondrial pyruvate metabolism and MPC function.

We observed distinct mechanisms by which the C289T and T236A *MPC1* alleles cause MPC deficiency. The *MPC1* C289T allele truncated A58G protein failed to stabilize MPC2 and form MPC complexes. The *MPC1* C289T allele full-length R97W protein was less stable but, when overexpressed, formed complexes with MPC2 that retained pyruvate transport activity. Conversely, the *MPC1* T236A allele L79H protein formed stable complexes with MPC2, but these complexes failed to transport pyruvate. These findings inform MPC structure-function relationships and delineate three distinct biochemical pathologies resulting from two human patient *MPC1* mutations. This investigation also demonstrates an efficient molecular genetic system using the mouse C2C12 cell line to mechanistically investigate human inborn errors in pyruvate metabolism.

Results

Patient information. Four human patients harboring homozygous *MPC1* mutations from three different families have been previously reported (Table 1, refs. 7, 8, and Supplemental Figure 1; supplemental material available online with this article; https://doi.org/10.1172/jci.insight.126132DS1). Patient 1 (Family 1) is homozygous for the C289T *MPC1* mutation predicted to generate transcripts encoding full-length R97W and truncated A58G MPC1 proteins. Her symptoms and disease progression until death at age 19 months were previously described (8). Patient 2 (Family 2), Patient 3 (Family 3), and Patient 4 (Family 3) are homozygous for the T236A *MPC1* mutation encoding full-length MPC1 L79H protein (7). Patient 2 showed delayed psychomotor functions, seizures, and elevated serum levels of lactate and pyruvate. Patient 3 is a male who displayed peripheral neuropathy, cognitive disability, and visual impairment. Patient 4 is a female who showed mild developmental delays compared with her brother. Interaction of patients with reporting physicians is infrequent and additional information is not available.

Measurements of MPC1 and MPC2 protein content in patient fibroblasts. *MPC1* patient mutations, transcript structures, and protein conservation are shown in Figure 1A. Notably, and as previously reported, all patient mutations change strongly conserved amino acid residues (7). When *MPC1* patient mutations were initially reported, antibodies to detect MPC1 and MPC2 protein were not available. How these mutations affect MPC protein levels and complex formation remains incompletely understood. We performed Western blots to compare MPC1 and MPC2 protein levels in human telomerase reverse transcriptase (hTERT) lifespan extended control and patient fibroblasts (7). In cells harboring the *MPC1* C289T mutation, both MPC1 (Figure 1, B and C) and MPC2 (Figure 1, B and D) decreased. Conversely, in cells harboring the *MPC1* T236A mutation, MPC1 protein was retained (Figure 1, B and C) and MPC2 protein was only partially lost (Figure 1, B and D). Compared with control fibroblasts, *MPC1* C289T transcript levels were decreased by nearly half, whereas *MPC1* T236A transcript levels were not different (Figure 1E). Thus, changes in *MPC1* transcript levels could not explain the loss of MPC1 protein in C289T patient fibroblasts.

Table 1. Summary of patient information from three consanguineous families

	Patient 1[A] (Family 1)	Patient 2[B] (Family 2)	Patient 3[B] (Family 3)	Patient 4[B] (Family 3)
Degree of consanguinity	1st cousin	1st cousin	1st cousin	1st cousin
Sex of the affected individuals	Female	Male	Male	Female
Age	19 months (deceased)	~20 years	~17 years	~12 years
Genetic change	c.289C→T	c.236TA	c.236T→A	c.236T→A
Allelic genotype	Homozygous	Homozygous	Homozygous	Homozygous
Predicted protein change	p.Arg^{97}→Trp(R97W) and Ala^{58}Gly followed by a frameshift of 2 DNA base pairs leading to a premature stop codon (A58GfsX2)	p.Leu^{79}→His(L79H)	p.Leu^{79}→His(L79H)	p.Leu^{79}→His(L79H)
Pregnancy	Complicated	Uneventful	Intrauterine growth retardation	Uneventful
Phenotype	Facial dysmorphism, respiratory distress, severe lactic acidosis, cerebral atrophy, periventricular leukomalacia with calcifications, neurological deterioration, and death	Psychomotor retardation, developmental delay from birth, hypotonia, seizures	Peripheral neuropathy, cognitive disability, visual impairment	Milder developmental delay and same biochemical features as her brother
Developmental delay	Severe	Mild	Severe	Mild
Serum finding	Hyperlactacidemia, hyperpyruvicemia normal, lactate-pyruvate ratio	Mild hyperlactacidemia, hyperpyruvicemia, Mild hyperlactacidemia, hyperpyruvicemia, normal lactate-pyruvate ratio	Mild hyperlactacidemia, hyperpyruvicemia, normal lactate-pyruvate ratio	
Treatment	Ketogenic diet (metabolic acidosis not corrected)	Ketogenic diet	Ketogenic diet	Ketogenic diet

[A]Clinical information (8) and genetic analysis (7) were previously published. [B]Minimal clinical information and genetic analysis were previously reported (7). Maternal pregnancy condition, developmental status, and serum findings not previously reported. Current degree of patient adherence to ketogenic diet is unknown.

MPC2 transcript levels were increased in *MPC1* C289T cells, consistent with counterregulation for loss of MPC proteins, but unchanged in *MPC1* T236A cells (Figure 1F). The persistence of MPC proteins in *MPC1* T236A versus C289T cells was surprising given that both mutations result in a similar loss of pyruvate oxidation (7, 22).

Generation and characterization of MPC1-knockout C2C12 cells. We aimed to develop an efficient molecular genetic system for examining the relationship between *MPC1* patient mutations and function. Compared with human fibroblasts, even hTERT lifespan extended, the mouse C2C12 myoblast cell line is immortal, proliferates rapidly, and, importantly, oxidizes pyruvate at high rates (23). This allows timely generation of stable, genetically modified cell lines facilitating high signal-to-noise measurements of pyruvate metabolism. We first aimed to generate Δ*Mpc1* C2C12 lines for subsequent complementation with and functional testing of *MPC1* patient alleles. CRISPR/Cas9 was utilized to delete from within the *Mpc1* 5′-UTR to beyond the translation start codon (Figure 2A). Immunoblotting confirmed that CRISPR/Cas9 *Mpc1* disruption ablated MPC1 protein expression (Figure 2, B and C). Consistent with other published data (11, 12), MPC1-knockout cells (Δ*Mpc1*) expressed normal levels of *Mpc2* mRNA but undetectable levels of MPC2 protein (Figure 2, B and D, and Supplemental Figure 2, A and B).

To measure MPC activity directly, mitochondria were purified from WT and Δ*Mpc1* cells and tested for [2-^{14}C]-radiolabeled pyruvate uptake activity (24). *Mpc1* deletion resulted in loss of mitochondrial pyruvate uptake (Figure 2E). To examine mitochondrial function, NADH-linked, complex I–dependent cellular respiration was measured using pyruvate and glutamine as substrates. *Mpc1* deletion strongly impaired pyruvate-driven respiration (Figure 2F). However, levels of glutamine-driven respiration were similar between WT and Δ*Mpc1* cells (Figure 2G). This is consistent with Δ*Mpc1* C2C12 cells having a specific defect in mitochondrial pyruvate transport rather than a global metabolic impairment.

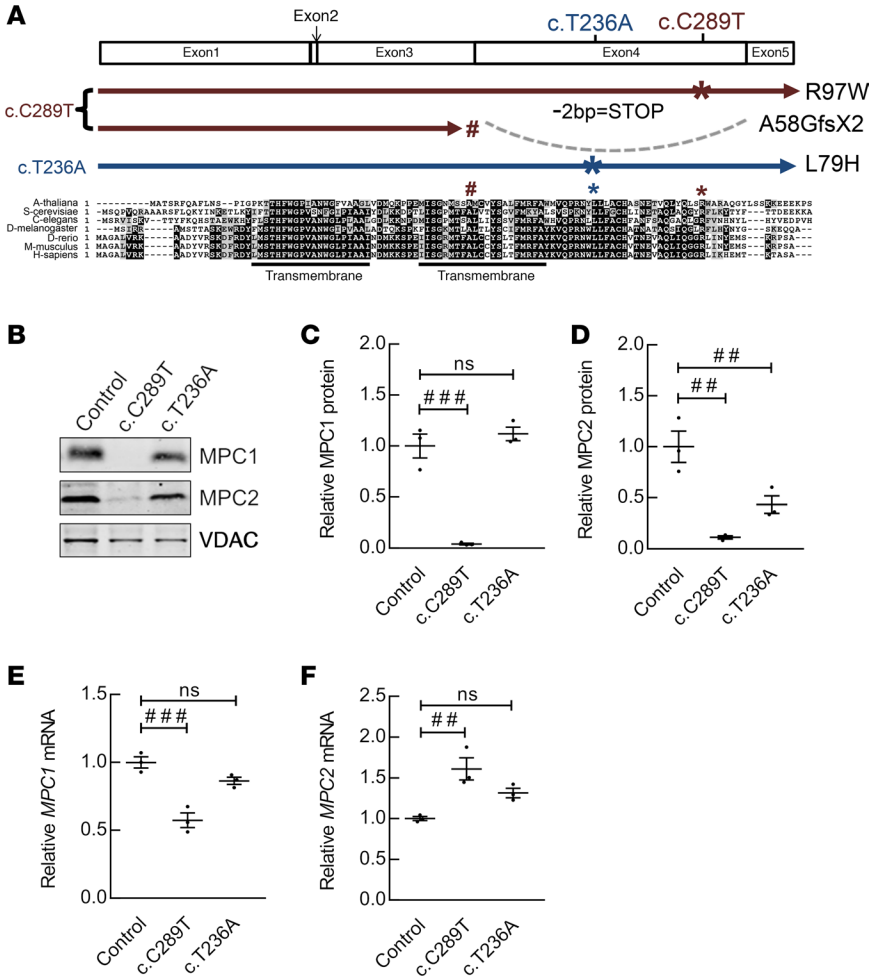

Figure 1. Patient fibroblasts contain *MPC1* mutations on highly conserved residues and express aberrant MPC1 and MPC2 levels. (**A**) Schematic of *MPC1* transcript indicating location of patient mutations. The c.C289T mutation produces 2 mRNAs shown as red arrows: a full-length transcript (R97W), and a truncated transcript (A58GfsX2). The c.T236A mutation coding for L79H is shown as a blue arrow. Sequence alignments show evolutionary conservation across multiple species. Two transmembrane regions were predicted using transmembrane helix prediction (TMHMM). MPC1 point mutations are marked by *, and truncated MPC1 mutant is indicated with #. (**B**) Representative MPC1, MPC2, and VDAC levels visualized by immunoblot of immortalized patient fibroblasts from Control, c.C289T, or c.T236A mutants (n = 3). (**C** and **D**) Quantification of relative MPC1 (**C**) and MPC2 (**D**) protein levels relative to VDAC in patient fibroblasts c.C289T and c.T236A as compared with WT (n = 3). (**E** and **F**) Relative *MPC1* (**E**) and *MPC2* (**F**) mRNA levels in patient fibroblasts c.C289T and c.T236A as compared with WT (n = 3). Data are presented as mean ± SEM. One-way ANOVA was performed for **C**–**F** ($^{\#\#}P \le 0.01$, $^{\#\#\#}P \le 0.001$, ns = not significant; see also Supplemental Figure 1).

MPC1 C-terminal truncation causes MPC-complex instability and dysfunction. To examine the suitability of *MPC1*-complemented Δ*Mpc1* C2C12 cells for detecting dysfunctional *MPC1* alleles, we performed proof-of-concept testing. Previous reports have shown that both MPC1 and MPC2 proteins are obligate for stabilizing each other and thus the MPC complex (7–9, 22, 23). We reasoned that a functional MPC1 protein would interact with and stabilize MPC2 in Δ*Mpc1* cells. Δ*Mpc1* cells were transduced with a series of constructs encoding increasingly C-terminally truncated MPC1 protein. Complemented lines were examined by Western blot for MPC1 protein expression and rescue of endogenous MPC2 protein expression. Complementation with WT human MPC1 rescued endogenous MPC2 protein to native levels and thus stabilized the MPC complex (Figure 3, A–C). MPC2 protein rescue was significantly decreased when MPC1 was truncated by 9 amino acids (ΔC9) and became nearly unobservable when truncation reached 18 amino acids (ΔC18; Figure 3, A–C). These data demonstrate that the MPC1 C-terminus is important for stabilizing MPC1, MPC2, and thus the MPC complex.

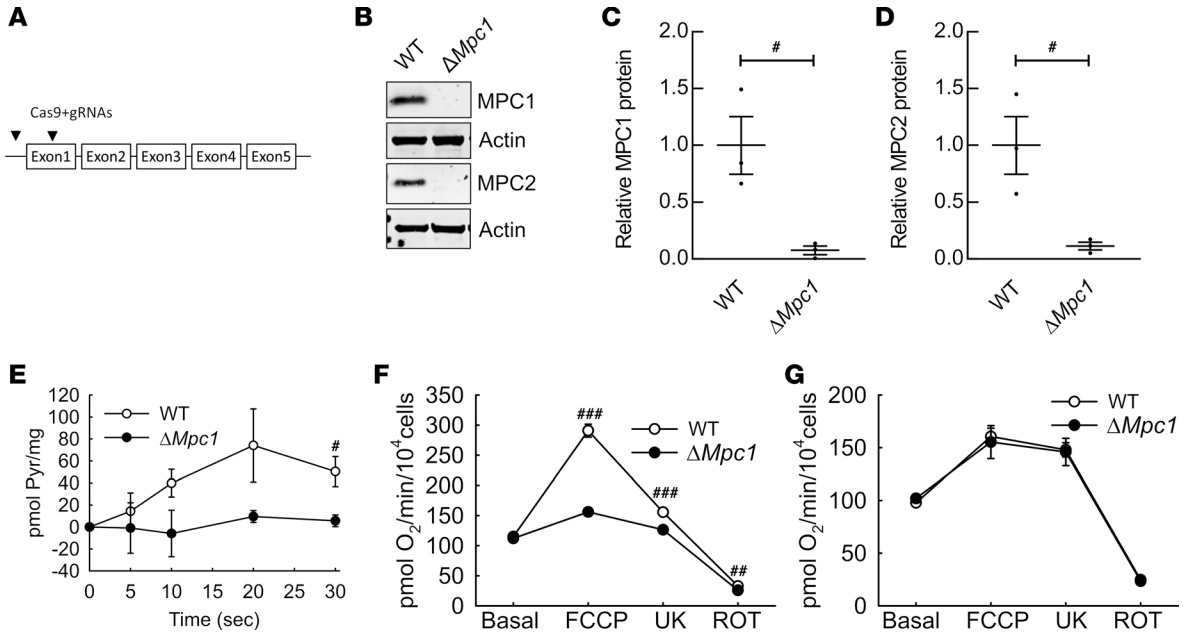

Figure 2. Generation and characterization of MPC1-knockout cell lines (Δ*Mpc1*). (**A**) Schematic displaying CRISPR sgRNA locations used to generate Δ*Mpc1* cell lines. (**B**) Representative MPC1, MPC2, and actin levels visualized by immunoblot in WT C2C12 following transduction with an empty vector (WT) or sgRNAs targeting Mpc1 (Δ*Mpc1*) (n = 3). (**C** and **D**) Quantification of relative MPC1 (**C**) and MPC2 (**D**) protein levels relative to actin in WT and Δ*Mpc1* cells (n = 3). (**E**) [2-^{14}C]-radiolabeled pyruvate uptake of mitochondria isolated from WT and Δ*Mpc1* cells (n = 4). (**F** and **G**) Respiration driven by 10 mM pyruvate (**F**) and 10mM glutamine (**G**) in WT and Δ*Mpc1* cells (n = 12, 3 clonal lines/genotype × 4 replicates/clonal line). Pyr, pyruvate; UK, UK5099; ROT, rotenone; FCCP, carbonyl cyanide-4-(trifluoromethoxy)phenylhydrazone. Data are presented as mean ± SEM. Two-tailed unpaired t test was performed for **C**–**G** ($^{\#}P \le 0.05$, $^{\#\#}P \le 0.01$, $^{\#\#\#}P \le 0.001$; see also Supplemental Figure 2).

We considered that MPC-complex stability may not be synonymous with MPC pyruvate transport activity. To address this, we compared WT and complemented Δ*Mpc1* C2C12 cells by pyruvate oxidation assays. Complementation with WT human MPC1 restored pyruvate-driven respiration to WT C2C12 levels (Figure 3, D and E, and Supplemental Figure 3 for non-normalized respiration data). MPC1 C-terminally truncated by 12 (ΔC12) or 18 (ΔC18) amino acids failed to rescue carbonyl cyanide-4-(trifluoromethoxy)phenylhydrazone–stimulated (FCCP-stimulated), pyruvate-driven respiration (Figure 3, D and E, and Supplemental Figure 3 for non-normalized respiration data). Taken together, the rescue data demonstrate that complementation of human *MPC1* alleles in Δ*Mpc1* mouse C2C12 cells enables detection of abnormalities in MPC-complex formation and function.

MPC1 patient mutations differentially affect MPC-complex stability and activity. To understand the distinct effects of each *MPC1* patient mutation on MPC biochemical function, Δ*Mpc1* mouse C2C12 cells were complemented with WT and patient *MPC1* alleles, and changes in MPC1 and MPC2 protein levels were measured. Ectopically expressed WT MPC1 and MPC1 L79H protein reached similar levels (Figure 4, A and B). In contrast, the full-length MPC1 R97W protein expression level was significantly lower and truncated MPC1 A58G protein was undetectable (Figure 4, A and B). As observed in experiments complementing Δ*Mpc1* cells with truncated MPC1 proteins, complementation with MPC1 WT rescued MPC2 protein to endogenous levels. Moreover, MPC1 L79H and R97W proteins also rescued MPC2 to endogenous levels. In contrast, expressing truncated MPC1 A58G protein did not (Figure 4, A and C).

To account for potential differences in antibody affinities for mouse, human, and mutated human MPC proteins, we performed additional control experiments. Parallel complementation experiments were performed in human embryonic kidney (HEK) 293T cells lacking MPC1 protein (Δ*MPC1*). Results were highly similar to our observations in mouse C2C12 cells. Compared with endogenous WT MPC1 protein, complemented WT and L79H MPC1 proteins were expressed at high levels, whereas R97W and A58G proteins were, respectively, expressed at low and undetectable levels (Supplemental Figure 4, A and B). MPC2 protein was rescued to endogenous levels by L79H and R97W but not by truncated A58G protein constructs (Supplemental Figure 4, A and C).

To rule out antibody epitope mutation as causing low detectable levels of R97W and the apparent

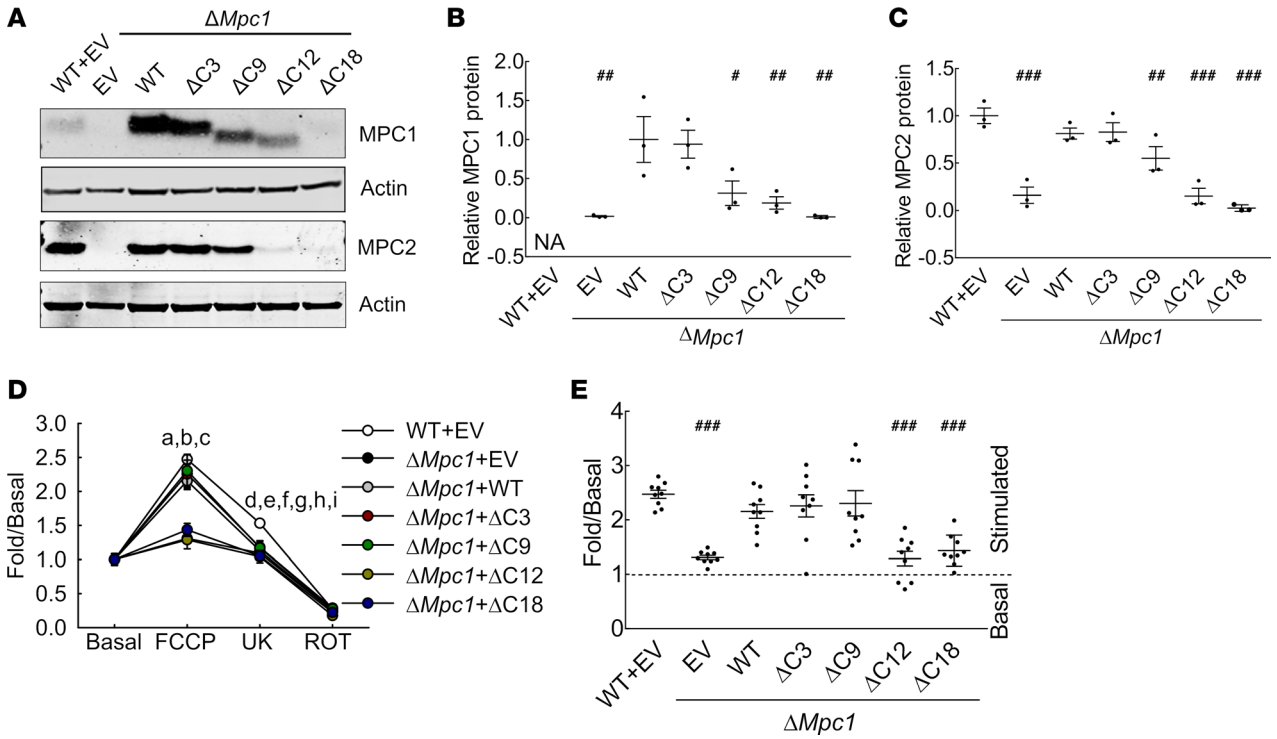

Figure 3. MPC1 C-terminal truncation causes MPC-complex instability and dysfunction. (**A**) Representative MPC1, MPC2, and actin levels visualized by immunoblot in WT C2C12 transduced with a guideless Cas9 vector and subsequently with an empty vector (WT+EV) compared Δ*Mpc1* cells complemented with empty vector (EV), WT human MPC1 (WT), or MPC1 mutants C-terminally truncated by 3 (ΔC3), 9 (ΔC9), 12 (ΔC12), or 18 amino acids (ΔC18) (n = 3). (**B** and **C**) Quantification of relative MPC1 (**B**) and MPC2 (**C**) protein levels relative to actin, statistics versus Δ*Mpc1*+WT (**B**) or WT+EV (**C**) (n = 3). (**D**) Respiration driven by 10 mM pyruvate of cell lines described in **A**. Letters represent significant differences in FCCP-stimulated respiration among Δ*Mpc1*+EV, Δ*Mpc1*+ΔC12, Δ*Mpc1*+ΔC18 (a–c; $P \leq 0.001$) versus WT+EV, and in UK5099-inhibited respiration among Δ*Mpc1*+EV, Δ*Mpc1*+WT, Δ*Mpc1*+ΔC12, Δ*Mpc1*+ΔC18 (d–g; $P \leq 0.001$), and Δ*Mpc1*+ΔC3, Δ*Mpc1*+ΔC9 (h and i; $P \leq 0.01$) versus WT+EV (n = 9; 3 clone lines/genotype × 3 technical replicates/clone line). (**E**) Quantification of FCCP-stimulated normalized to basal pyruvate-driven respiration by complemented Δ*Mpc1* cell lines as compared with WT+EV (n = 9; 3 clone lines/genotype × 3 technical replicates/clone line). Data are presented as mean ± SEM. One-way ANOVA was performed for **B**–**E** ($^{\#}P \leq 0.05$, $^{\#\#}P \leq 0.01$, $^{\#\#\#}P \leq 0.001$; see also Supplemental Figure 3).

absence of truncated A58G protein, we expressed patient MPC1 proteins with a C-terminal FLAG epitope tag. Immunoblotting confirmed that the R97W protein accumulated at a lower level whether detected with anti-MPC1 or anti-FLAG antibodies (Supplemental Figure 4, D and E). Importantly, the truncated MPC1 A58G protein was not detectable by either antibody, demonstrating that it is intrinsically unstable (Supplemental Figure 4, D and E). Expressing WT-FLAG or L79H-FLAG rescued MPC2 protein to endogenous levels, whereas expressing R97W-FLAG only partly restored MPC2 protein expression levels (Supplemental Figure 4, D and F). Truncated MPC1 A58G-FLAG protein expression was unable to rescue MPC2 protein content (Supplemental Figure 4, D and F). These results show that the MPC1 L79H mutant protein forms a stable complex with MPC2, that MPC1 R97W protein is less stable, and that truncated MPC1 A58G protein is unstable and leads to equivalent MPC2 degradation.

Because a stable MPC complex is not necessarily competent for pyruvate transport activity, we tested the effect of patient mutations on MPC function by measuring pyruvate-driven respiration in complemented Δ*Mpc1* C2C12 cells. Complementation with WT and R97W MPC1 proteins rescued pyruvate-driven respiration (Figure 4, D and E, and Supplemental Figure 5A for non-normalized respiration data). A58G MPC1 protein showed no rescue of pyruvate-driven respiration (Figure 4, D and E). However, interestingly, though L79H was stable and rescued MPC2 protein expression, it failed to restore pyruvate-driven respiration (Figure 4, D and E). Results were similar when respiration was measured with 1 mM pyruvate and FCCP concentrations of 0.1 μM, 0.33 μM, and 1 μM (Supplemental Figure 5, B–G). This indicates that clonal differences in non–MPC-facilitated mitochondrial pyruvate oxidation and FCCP dosing were not driving pyruvate oxidation differences ascribed to patient alleles.

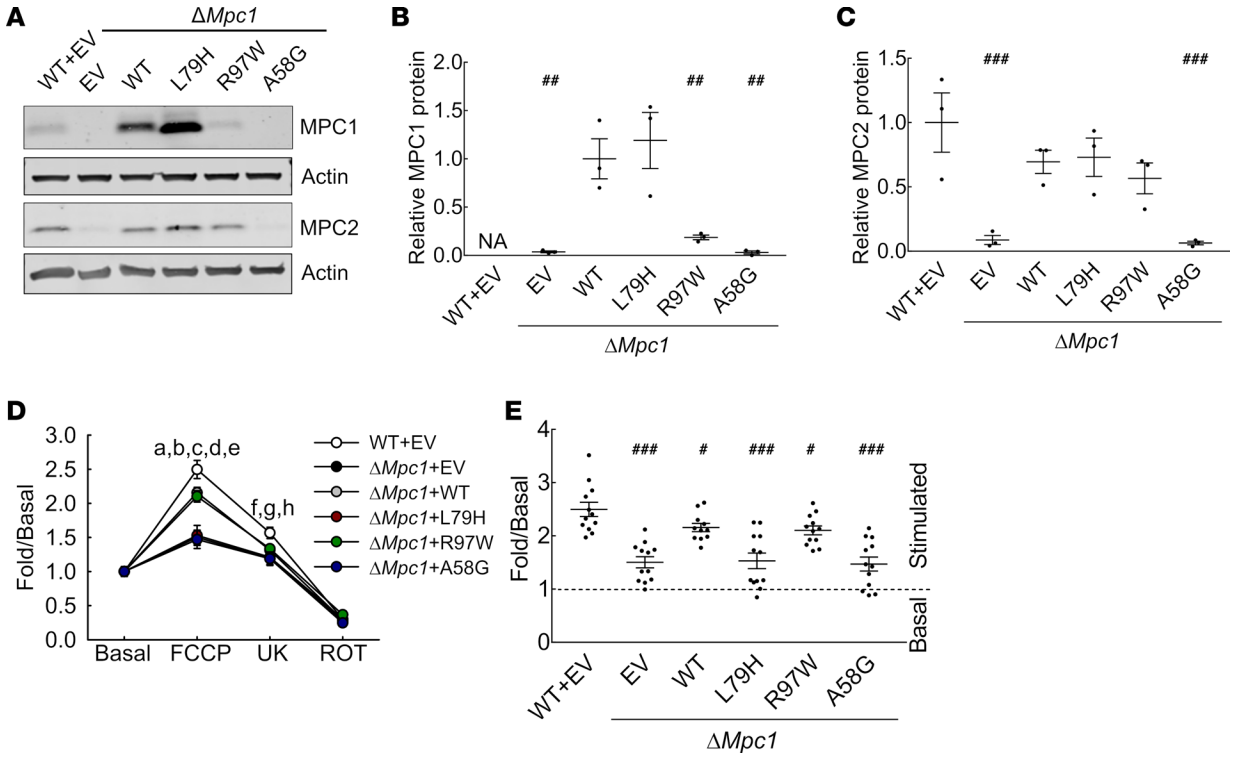

Figure 4. MPC1 patient mutations display varied MPC complex stability and activity. (**A**) Representative MPC1, MPC2, and VDAC with Actin levels visualized by immunoblot in WT C2C12 cells transduced with guideless Cas9 vector and subsequently with an empty vector (WT+EV) compared with Δ*Mpc1* cells complemented with an empty vector (EV), WT human MPC1 (WT), or MPC1 mutants (L79H, R97W, and A58G) (n = 3). (**B** and **C**) Quantification of MPC1 (**B**) and MPC2 (**C**) protein levels relative to Actin, statistics versus Δ*Mpc1*+WT (**B**) or WT+EV (**C**) (n = 3). (**D**) Respiration driven by 10 mM pyruvate of cell lines described in **A**. Letters represent a significant difference in FCCP-stimulated respiration among Δ*Mpc1*+EV, Δ*Mpc1*+L79H, Δ*Mpc1*+A58G (a–c; $P \le 0.001$) and Δ*Mpc1*+WT, Δ*Mpc1*+R97W (d and e, $P \le 0.05$) versus WT+EV, and in UK5099-inhibited respiration among Δ*Mpc1*+EV and Δ*Mpc1*+L79H, Δ*Mpc1*+A58G (f–h; $P \le 0.01$) versus WT+EV (n = 12; 2 clone lines/genotype × 6 technical replicates/clone line). (**E**) Quantification of FCCP-stimulated normalized to basal pyruvate-driven respiration by complemented Δ*Mpc1* cell lines as compared with WT+EV (n = 12; 2 clone lines/genotype × 6 technical replicates/clone line). Data are presented as mean ± SEM. One-way ANOVA was performed for **B**–**E** ($^{\#}P \le 0.05$, $^{\#\#}P \le 0.01$, $^{\#\#\#}P \le 0.001$; see also Supplemental Figures 4 and 5).

MPC1 T236A results in stable but transport incompetent MPC complexes. The result that MPC1 L79H protein fully stabilized MPC2 protein but failed to rescue pyruvate-driven respiration in *Mpc1* C2C12 cells could be potentially explained by mechanisms other than loss of MPC transport activity. Because respiration experiments utilize oxygen consumption as the read-out, other enzymes in pyruvate metabolism such as pyruvate dehydrogenase (PDH) and pyruvate carboxylase (PC) may influence pyruvate-driven respiration. We considered the possibility that the MPC1 L79H protein mutation impairs respiration by disrupting pyruvate channeling mechanisms, such as through PDH or PC, rather than ablating MPC transport activity. We directly measured L79H MPC activity by measuring isolated mitochondria [2-^{14}C]-radiolabeled pyruvate uptake. In corroboration with respiration assays, Δ*Mpc1* C2C12 cell mitochondria did not transport pyruvate, but complementation with WT human MPC1 restored pyruvate uptake activity to WT C2C12 cell levels. Remarkably, mitochondria purified from MPC1 L79H–complemented Δ*Mpc1* C2C12 cells did not take up pyruvate (Figure 5A). This demonstrates that the L79H MPC1 mutation impairs pyruvate-driven respiration by ablating MPC pyruvate transport activity.

To understand whether MPC1 L79H ablates MPC activity by disrupting mitochondrial targeting, we performed cellular fractionation and Western blot analysis of *ΔMpc1* cells complemented with WT and L79H MPC1 proteins. We found that L79H protein was enriched in the mitochondrial fraction, as was MPC1 WT (Supplemental Figure 6A). We extended this to tryptic mitochondrial digests, with and without detergent, to allow trypsin to access inner mitochondrial membrane proteins. MPC1 L79H was digested with the presence but not absence of detergent, consistent with proper targeting to the inner mitochondrial membrane (Supplemental Figure 6B).

Because MPC1 L79H forms stable, mitochondrially targeted complexes with MPC2, we considered whether MPC1 L79H could exert dominant negativity. This is an important clinical consideration because

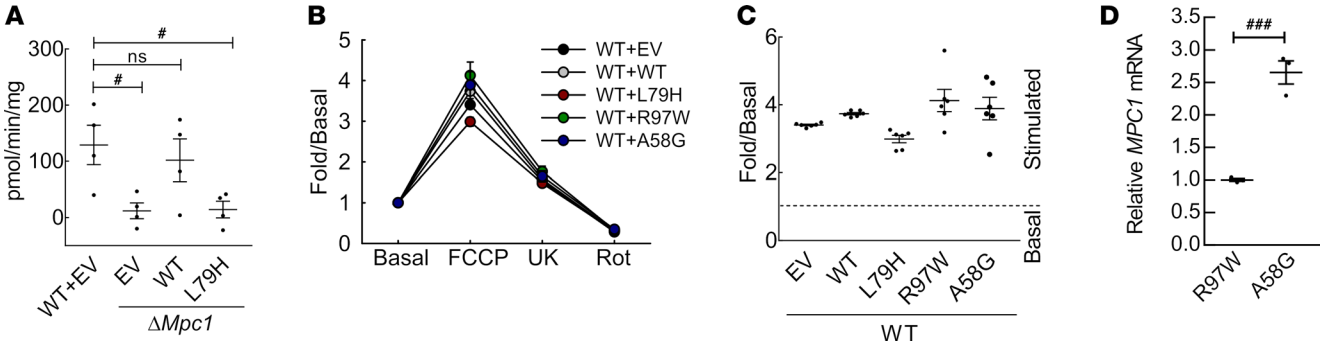

Figure 5. MPC1 patient mutations affect MPC activity. (**A**) [2-^{14}C]-radiolabeled pyruvate uptake of mitochondria isolated from WT (WT+EV) and Δ*Mpc1* cells complemented with an empty vector (EV), human MPC1 (WT), or MPC1-L79H mutant (L79H) (n = 4). (**B**) Respiration driven by 10 mM pyruvate in WT C2C12 cell lines complemented with an empty vector (EV), WT human MPC1 (WT), or MPC1 mutants (L79H, R97W, and A58G) (N = 6; parental polyclonal line × 6 technical replicates). (**C**) Quantification of FCCP-stimulated normalized to basal pyruvate-driven respiration by complemented WT cell lines (n = 6; parental polyclonal line × 6 technical replicates). (**D**) Quantification of *MPC1* (R97W) and *MPC1* (A58G) mRNA in patient fibroblasts harboring the c.C298T MPC1 mutation (n = 3). Data are presented as mean ± SEM. One-way ANOVA was performed for **A**–**D** ($^{\#}P \le 0.05$, $^{\#\#\#}P \le 0.001$, ns = not significant; see also Supplemental Figures 6 and 7).

patients heterozygous for this mutation could carry metabolic impairments and thus health risks that might not be readily detectable with basic observation. To test for MPC1 L79H dominant negativity, we ectopically expressed WT and mutant patient MPC1 protein in WT C2C12 cells. WT C2C12 cells overexpressing WT, L79H, R97W, and truncated A58G MPC1 protein did not display significant differences in pyruvate-driven respiration (Figure 5, B and C, and Supplemental Figure 6C for non-normalized respiration data). Thus, in the context of endogenous, WT MPC1 expression, overexpression of the dysfunctional MPC1 L79H protein did not exert dominant negativity. This is consistent with the apparent normal health of family members heterozygous for the *MPC1* T236A allele encoding the MPC1 L79H protein (7).

MPC1 C289T results in unstable truncated major and full-length minor MPC1 protein variants. Because complementing *ΔMpc1* cells with *MPC1* C289T cDNA encoding the full-length R97W but not the truncated A58G protein rescued MPC function, we further considered how the relative abundance of these transcripts in patient fibroblasts could explain the loss of MPC2 protein and MPC function. By quantitative PCR (qPCR) we measured the relative abundance of full-length R97W and truncated A58G transcripts in the *MPC1* C289T patient fibroblasts. The R97W transcript was detected but at a markedly lower level compared with the A58G transcript (Figure 5D). Treatment with neither MG132 to inhibit the proteasome nor bafilomycin to inhibit autophagy led to MPC1 or MPC2 accumulation in *MPC1* C289T patient fibroblasts (Supplemental Figure 7, A and B), consistent with MPC1 and MPC2 protein degradation by mitochondrial proteases.

To rule out that the lower level of MPC1 R97W protein in complemented Δ*Mpc1* C2C12s was not due to lower *MPC1* transcript levels, we quantified relative abundance of complemented human *MPC1* transcripts (Supplemental Figure 7C). Complemented R97W transcript levels were not less than complemented WT and L79H transcript levels and exceeded endogenous mouse transcript levels. This indicates that the lower level of complemented R97W protein is a not a result of decreased mRNA. To test whether the R97W protein is less efficiently translated, we transfected HEK 293T cells with plasmids encoding MPC1 WT, L79H, and R97W with and without mutation of the start methionine to valine followed by a P2A-GFP sequence. A P2A element induces ribosome skipping and, in contrast to an internal ribosome entry site (IRES), results in translation of the second cDNA sequence that is dependent on translation of the first cDNA sequence. Mutation of the MPC1 WT, L79H, and R97W start codon similarly decreased reporter GFP protein content measured by flow cytometry (Supplemental Figure 7D), consistent with similar translational efficiency. Combined with qPCR results from patient fibroblasts and complemented Δ*Mpc1* C2C12 cells, these data indicate the lack of detected R97W protein in patient fibroblasts results from both decreased transcript levels and protein instability.

WT MPC complexes predominate when WT and L79H MPC1 are coexpressed. We hypothesized that when MPC1 WT and mutant MPC1 L79H proteins are both present WT MPC complexes predominate, leading to MPC sufficiency. To drive stoichiometrically equal expression of MPC1 WT and L79H proteins, we subcloned both cDNAs into the same expression vector under control of the same promoter but separated by a P2A element. In contrast to an IRES, A P2A element does not result in decreased translation of the second cDNA. MPC1 WT was C-terminally tagged with hemagglutinin (HA), while MPC1 L79H was C-terminally tagged with FLAG.

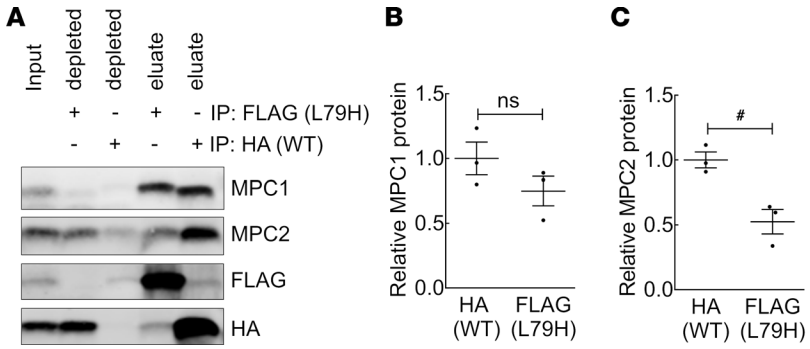

Figure 6. The MPC1(L79H)-MPC2 interaction is weaker than MPC1(WT)-MPC2. (**A**) Representative MPC1, MPC2, FLAG, and HA levels visualized by immunoblot of input, immune-depleted (depleted), wash, and eluate fractions from coimmunoprecipitation of MPC1 proteins (L79H-FLAG or MPC1-HA) precipitated using FLAG or HA antibody in the Δ*Mpc1* cell line expressing both MPC1-HA and L79H-FLAG ($n = 3$). Quantification of relative MPC1 (**B**) and MPC2 (**C**) levels in eluates from L79H-FLAG and MPC1-HA pull-downs ($n = 3$). Data are presented as mean ± SEM. Two-tailed unpaired *t* test was performed for **B** and **C** ($^{\#}P \leq 0.05$, ns = not significant; see also Supplemental Figure 8).

Coimmunoprecipitations by HA and FLAG showed similar levels of MPC1 WT and MPC1 L79H immunodepletion and retrieval in eluates (Figure 6, A and B). Importantly, compared with MPC1 L79H (FLAG), pull-down of MPC1 WT (HA) coimmunoprecipitated a greater fraction of endogenous MPC2 protein. This indicates that when transcriptional and translational drive for MPC1 WT and L79H protein expression are equal then MPC1 WT forms more complexes with MPC2 (Figure 6, A and C). To test for nonspecific effects of FLAG and HA tags, coimmunoprecipitation experiments were performed with the tags switched (Supplemental Figure 8, A–C). Results were similar, with more MPC2 coimmunoprecipitated by MPC1 WT (FLAG) than MPC1 L79H (HA).

Taken together, several of our observations suggest that MPC1 WT protein competitively excludes MPC1 L79H protein from association with MPC2 protein. First, expressing only MPC1 WT or MPC1 L79H in Δ*Mpc1* C2C12 cells equally restabilizes MPC2 protein. Second, because the overexpression system used here generates excess MPC1 WT and L79H proteins, neither is stoichiometrically limiting for complexation to MPC2. Third, when MPC1 L79H is overexpressed in WT C2C12 cells normal pyruvate oxidation persists. Fourth, human patients heterozygous for MPC1 L79H are asymptomatic and inheritance appears to be autosomal recessive (8).

Discussion

Pyruvate is a key metabolite that links the cytoplasmic process of glycolysis to mitochondrial respiration and TCA cycle–dependent biosynthesis. Thus, it is not surprising that deranged pyruvate metabolism contributes to a host of diseases (6). Since the molecular identification of the genes encoding the MPC (7, 9), an increasing number of investigations have demonstrated the prominent role of mitochondrial pyruvate uptake in regulating cellular and organismal biology (11, 12, 15, 23, 25–27). Here, we demonstrate that 2 *MPC1* mutations identified in human patients with inborn errors in pyruvate metabolism cause MPC dysfunction by three different mechanisms.

We observed that the *MPC1* C289T mutation causes MPC insufficiency by loss of the MPC complex. Western blots of human patient fibroblasts harboring the C289T *MPC1* mutation, which generates transcripts encoding both the full-length R97W and truncated A58G MPC1 proteins (7), showed near total loss of MPC1 and MPC2 proteins. Similarly, complementing Δ*Mpc1* C2C12 cells with cDNA encoding the truncated MPC1 A58G protein, with or without a C-terminal FLAG tag, failed to result in detectable MPC1 expression or MPC2 rescue. In contrast, complementation with full-length MPC1 R97W, compared with MPC1 WT, resulted in minimally detectable MPC1 protein expression and nearly complete rescue of MPC2 protein levels. The difference in MPC1-to-MPC2 ratios following complementation with MPC1 WT versus MPC1 R97W suggests that MPC1 R97W instability is ameliorated once complexed with MPC2. In this case, overexpression overcomes MPC1 R97W instability, sustaining a pool size sufficient to complex with available MPC2. Thus, the finding that complementation with MPC1 R97W restored pyruvate-driven respiration is likely a result of overexpression. This helps explain why detected endogenous full-length MPC1 R97W tran-

script does not result in MPC2 protein accumulation in human fibroblasts. Together, these data demonstrate that the *MPC1* C289T allele causes MPC insufficiency primarily by missplice-driven encoding of the truncated MPC1 A58G protein and secondarily by decreased stability of the full-length MPC1 R97W protein.

Whereas *MPC1* C289T results in MPC-protein-complex loss, we found, surprisingly, that *MPC1* T236A results in a stable MPC1 L79H–MPC2 complex lacking pyruvate transport activity. Thus, MPC1 L79H is an inactivating mutation. This demonstrates that MPC-complex formation is not synonymous with pyruvate transport activity. The MPC-complex structure remains unsolved, leaving the precise membrane topology and specific residues catalyzing transport unknown. Biochemical experiments indicate MPC1 to have 2 transmembrane helices, with both the N- and C-termini projecting into the mitochondrial matrix (10, 28, 29). In humans and mice, MPC1 L79 is predicted to be in the C-terminal tail, 8 amino acid residues beyond the second transmembrane domain (28, 29). In silico modeling predicts L79 to be in the C-terminus facing the matrix (30). This residue is near amino acids G74 and P75, which are predicted to form hinges and provide structural flexibility facilitating R76 rotation (30). Having an aromatic ring–containing histidine residue instead of a hydrophobic leucine residue could reasonably change MPC1 structure and conformational repertoire. More intensive structural studies are required to fully understand how the L79H mutation disrupts pyruvate transport. Overall, our combined findings showing that MPC1 L79H is inactivating, that MPC1 R97W is destabilizing, and that MPC1 C-terminal truncations of 12 or more amino acids are severely destabilizing, demonstrate the MPC1 C-terminus to be critical for MPC function.

Interestingly, in contrast to the single human patient case reported for *MPC1* C289T, which led to early death (7, 8), homozygosity for the *MPC1* T236A allele encoding inactive MPC1 L79H protein is not lethal (7). We expect this difference is due to genetic heterogeneity in human populations that confer varying tolerance to MPC deficiency. Indeed, many mechanisms are reported to compensate for decreased MPC function, including increased glutaminolysis (11, 23), increased fatty-acid oxidation (23), ketogenic diet, and a pyruvate-alanine cycling MPC bypass (11, 12).

Notably, while MPC disruption during development is pathological, tissue-selective MPC disruption after development may have therapeutic value. Previous work clearly demonstrates the requirement of MPC1 and MPC2 in mammalian development. Both MPC1 and MPC2 mouse knockout models display embryonic lethality during midgestation (21, 31) and MPC1 hypomorphs caused early perinatal lethality (20). In contrast, postnatal liver-specific MPC disruption attenuates obesity-induced hyperglycemia (11, 12) and decreases fibrosis and inflammation in mouse models of nonalcoholic fatty liver disease (NAFLD) and NASH (14, 32). The contrast between the clearly pathological effects of whole-body MPC disruption during prenatal development versus potential therapeutic effects of liver MPC disruption after development highlights the need to better understand tissue-specific pyruvate metabolism across developmental stages.

Accurately treating inborn errors of metabolism requires understanding the pathological mechanisms of the underlying mutations. Thus, it is important to understand how *MPC1* mutations, like those previously described, disrupt MPC function. Our work highlights that accurately understanding genetic mechanisms of MPC dysfunction requires isolating distinct components of function, including MPC1 and MPC2 protein levels, MPC-complex formation, and MPC activity. Because MPC mutations have only recently been identified and appear to be rare, they are not routinely screened for as a cause of patient metabolic abnormalities. Given the recent molecular identification of the MPC, its likely human MPC disease mutations will continue to be discovered. Although our findings here do not suggest new approaches for treating congenital MPC deficiency, they may, in combination with future studies, contribute to improved diagnosis and management of future MPC deficiency cases. For example, they raise the possibility of MPC1 stabilization as a treatment for MPC deficiency resulting from destabilizing but not inactivating mutations like MPC1 R97W.

In conclusion, we demonstrate that 2 human *MPC1* mutations cause MPC deficiency by distinct mechanisms. The *MPC1* C289T mutation results in loss of the MPC complex, whereas, the *MPC1* T236A mutation results in an inactive MPC complex. These findings provide insight into the fundamental biochemical mechanisms regulating MPC function and molecular etiology of human patient MPC deficiency. This work also illustrates the usefulness of a molecular genetic system using the mouse C2C12 cell line, CRISPR/Cas9 gene disruption, and human gene complementation to investigate mechanisms underlying human inborn errors in pyruvate metabolism.

Methods

Cell culture. Human skin fibroblasts (HSFs) were isolated, immortalized, and selected for antibiotic resistance as previously described (7). HSFs were maintained in DMEM with 15% FBS, 2 mM Glutamax, and 1% Primocin. HEK 293T and C2C12 cell lines were purchased from ATCC and confirmed to be mycoplasma-free using the PlasmoTest Mycoplasma Detection Kit according to the manufacturer's instructions (InvivoGen). HEK 293T and C2C12 were maintained in DMEM with 10% FBS, 2 mM Glutamax, and 1% penicillin-streptomycin. After CRISPR/Cas9 editing, lines were maintained in DMEM with 10% FBS, 1 mM pyruvate, 2 mM glutamine, 2 mM Glutamax, 1 mM citrate, 50 μg/mL uridine and 1% penicillin-streptomycin. All cell lines were grown at 37°C in an atmosphere of 5% CO_2.

Immunoblotting. Cellular proteins were extracted with lysis buffer (62.5 mM Tris pH 6.8, 2% SDS (m/v), 10% glycerol (v/v), and 0.1 μM dithiothreitol) and quantified using the Pierce BCA Protein Assay Kit (Thermo Fisher Scientific). Equal amounts of protein lysates were prepared in Laemmli buffer and boiled at 95°C for 10 minutes. Lysates were resolved on 10% Tricine-SDS-PAGE gels using a Mini-PROTEAN Tetra Cell running system (Bio-Rad) and transferred onto nitrocellulose membranes using a Trans-Blot transfer system (Bio-Rad). Blots were incubated in primary antibodies: MPC1 (1:1,000; Cell Signaling Technology catalog 14462), MPC2 (1:1,000; Cell Signaling Technology catalog 46141), VDAC (1:1,000; Cell Signaling Technology catalog 4661), actin (1:3,000; Cell Signaling Technology catalog 3700 or 4970), FLAG (1:1,000, Cell Signaling Technology catalog 8146 or 14793), HA (1:1,000, Cell Signaling Technology catalog 3724 or 2367), succinate dehydrogenase antibody (SDHa) (1:1,000; Cell Signaling Technology catalog 5839), PDH E2/E3bp (1:1,000; Abcam catalog ab110333), Tom20 (1:1,000; Cell Signaling Technology catalog 42406), cytochrome *c* (1:1,000; Cell Signaling Technology catalog 11940), PDH (1:1,000; Cell Signaling Technology catalog 3205), IDH2 (1:1,000; Proteintech catalog 15932-1-AP), ubiquitin (FK2) (1:1,000; EMD Millipore catalog ST1200), LC3b (1:1,000; Cell Signaling Technology catalog 2775), and p62 (1:1,000; Sigma catalog P0067-200UL). Fluorescent secondary antibodies, goat-anti-rabbit DyLight 800 conjugate (1:10,000; Thermo Fisher Scientific catalog 35571), donkey anti-rabbit DyLight 680 conjugate (1:10,000; Thermo Fisher Scientific catalog SA5-10042), goat anti–mouse IgG (H+L) DyLight 680 conjugate (1:10,000; Thermo Fisher Scientific catalog PI35519), and goat anti–mouse IgG (H+L) DyLight 800 conjugate (1:10,000; Thermo Fisher Scientific catalog SA5-10176) were used to visualize the signal, which was imaged using the Li-Cor Odyssey CLx system (LI-COR Biosciences). The average density of MPC1, MPC2, Actin, and VDAC immunoblots was quantified by ImageJ. Actin and VDAC were used as loading controls.

qPCR. RNA was extracted using TRIzol (Thermo Fisher Scientific) or RNeasy Mini Kit (Qiagen). Equal amounts of RNA per sample were reverse transcribed using High-Capacity cDNA Reverse Transcription Kit (Applied Biosystems) followed by qPCR reactions using SYBR Green (Thermo Fisher Scientific). The primer sequences for human *U36B4* were forward 5′-CGAGGGCACCTGGAAAAC-3′ and reverse 5′-CACATTCCCCCGGATATGA-3′. The primer sequences for human *GAPDH* were forward 5′-ACATCGCTCAGACACCATG-3′ and reverse 5′-TGTAGTTGAGGTCAATGAAGGG-3′. The primer sequences to measure total human *MPC1* were forward 5′-GGACTATGTCCGAAGCAAGG-3′ and reverse 5′-AAATGTCATCCGCCCACTGA-3′. The primer sequences to measure human *MPC2* were forward 5′-TGTGTGCTGGATTGGCTGAT-3′ and reverse 5′-CCAAATAAACCCTGTAGCCATCAA-3′. The primer sequences specific for R97W *MPC1* transcript were forward 5′-GGACTATGTCCGAAGCAAGG-3′ and reverse 5′-GTCATCCAAATGTCATCCGC-3′. The primer sequences specific for A58G *MPC1* transcript were forward 5′-GAAGCAAGGATTTCCGGGAC-3′ and reverse 5′-GTCATCCAAATGTCATCCGC-3′.

The primer sequences for mouse *Mpc1* were forward 5′-AACTACGAGATGAGTAAGCGGC-3′ and reverse 5′-GTGTTTTCCCTTCAGCACGAC-3′. The primer sequences for mouse *Mpc2* were forward 5′-CCGCTTTACAACCACCCGGCA-3′ and reverse 5′-CAGCACACACCAATCCCCATTTCA-3′. The primer sequences for mouse *U36b4* were forward 5′-CGTCCTCGTTGGAGTGACA-3′ and reverse 5′-CGGTGCGTCAGGGATTG-3′.

Generation of ΔMpc1 cell lines and ΔMPC1 cell lines. To generate *Mpc1* deletion (Δ*Mpc1*) in C2C12 cell lines, CRISPR guide RNAs (gRNAs) targeting exon1 of *Mpc1* were subcloned into lentiCRISPR v2 (Addgene plasmid 52961), using BbsI sites, as previously described (33). gRNA sequences were 5′-GCGCTCCTACCGGTGCCCGA-3′ and 5′-GCCAACGGCACGGCCATGGC-3′. Lentiviral particles were made by transfecting HEK 293T (ATCC) with lentiCRISPR v2 expressing no gRNA or gRNA of interests, psPAX2 (Addgene plasmid 12260), and pDM2.G (Addgene plasmid 12259) using polyethylenimine (PEI). Virus was

collected 72 hours after transfection. An equal mixture of virus and culture media were used to transduce mouse myoblast C2C12 cell lines using 8 μg/mL of polybrene. Infected cells were selected with 2 μg/mL of puromycin for 3 days and then diluted to create monoclonal lines. Genomic DNA from monoclonal lines was extracted using QuickExtract DNA Extraction Solution (Epicentre) according to the manufacturer's protocol and genotyped by PCR using the following primers: 5′-CTGCACTCGGTGACTCCATC-3′ and 5′-ACCATGTCTTTCAGTTCGCG-3′.

To generate Δ*MPC1* in 293T cell lines, CRISPR gRNAs targeting exon1 of *MPC1* were subcloned into the BbsI sites of pSpCas9(BB)-2A-GFP (PX458) (Addgene plasmid 48138). gRNA sequences were 5′-GGCGGACTATGTCCGAAGCA-3′ and 5′-GTGGCTCGCCGTCGGCTGCCG-3′. 293T cell lines were cotransfected with PX458 backbone lacking sgRNAs and PQCXIP backbone at 9:1 DNA ratio or cotransfection with PX458 harboring sgRNAs, and PQCXIP at a 4.5:4.5:1 ratio. Cells were selected using 2 μg/mL puromycin and monoclonally diluted. Cell lines were genotyped by PCR on extracted genomic DNA utilizing the following primers: 5′-CCTGTCATTGGCCGAGAGC-3′ and 5′-CCTCGTCGCGGACTGC-3′. MPC1 deletion was confirmed by Western blot.

Re-complementation of ΔMpc1 cell lines and ΔMPC1 cell lines. cDNA expressing human MPC1 [WT], C-terminally truncated MPC1 mutants (by 3 amino acids [ΔC3], 9 amino acids [ΔC9], 12 amino acids [ΔC12], or 18 amino acids [ΔC18], L79H [L79H], R97W [R97W], A58GfsX2 [A58G], and C-terminally FLAG-tagged versions of WT, L79H, R97W, A58G were subcloned into the PQCXIB vector (Addgene plasmid 17487) using NotI and BamHI sites. cDNA expressing L79H-FLAG P2A MPC1-HA P2A blasticidin resistance gene and L79H-HA P2A MPC1-FLAG P2A blasticidin resistance gene were also subcloned into the PQCXIB vector using NotI and EcoRV sites.

Retroviral particles were made by transfecting HEK 293T with PQCXIBs, VSV-G, and GagPol. The media were collected 72 hours after transfection and centrifuged at 1400 *g* for 5 minutes. Δ*Mpc1* cell lines were infected with equal mixtures of culture media and retrovirus expressing MPC1 proteins of interest and were selected with 10 μg/mL of blasticidin for 5 days.

Mitochondria isolation. In a procedure adapted from Bozidis et al. (34), cells were washed twice with PBS, pH 7.4, disassociated with 0.25% trypsin-EDTA (v/v), and resuspended in 10 mL culture medium per 15-cm^2 culture dish. Cell suspensions were collected in sterile 50-mL tubes and centrifuged at 200 *g* for 5 minutes at 4°C. Pelleted cells (300 mg) were resuspended in PBS, pH 7.4, and centrifuged for 5 minutes at 1,400 *g* at 4°C. The supernatant was removed, and the cell pellet was resuspended in 4 mL of MTE buffer (270 mM D-mannitol, 10 mM Tris-base, 0.1 mM EDTA, 1 mM PMSF, pH 7.4). Cell suspensions were lysed by sonication via 3 continuous pulses of 10 seconds each. Cell homogenates were centrifuged at 1,400 *g* for 10 minutes at 4°C to pellet cellular debris and nuclei. Supernatants were combined and crude mitochondria were pelleted by centrifugation at 15,000 *g* for 10 minutes at 4°C. The mitochondrial pellets were gently washed once with MTE buffer and kept on ice. The Bradford assay (Bio-Rad, 5000006) was used to quantify protein concentration (35).

Mitochondria pyruvate uptake assay. The pyruvate uptake protocol was based on a previously published method (24), with the following modifications. Crude mitochondria were diluted in 300 μLl of uptake buffer (120 mM KCl, 1 mM EGTA, 5 mM HEPES pH 7.4, 1 μM rotenone, and 1 μM Antimycin A). One hundred fifty microliters of diluted mitochondria were pretreated with 2 mM α-cyano-4-hydroxycinnamic acid (CHC) to inhibit MPC activity and act as negative uptake control. Twenty-five microliters of CHC-pretreated or untreated mitochondria were mixed with 25 μL of 2× pyruvate buffer (160 mM HEPES pH 6.1, 1 μM rotenone, 1 μM Antimycin A, 0.1 mM [2-^{14}C]-radiolabeled pyruvate, and 0.1 mM unlabeled pyruvate), generating a pH gradient to start and drive pyruvate uptake. After 30 seconds, 40 μL mitochondria (~100 μg per sample) was mixed with 100 μL stop buffer (uptake buffer, supplemented with 10 mM CHC and 40 mM HEPES pH 6.8). Mitochondria were transferred to a filtering apparatus composed of 0.8-μm cellulose and 0.45-μm nitrocellulose filters. Filters were washed twice with 140 μL of wash buffer (uptake buffer supplemented with 2 mM CHC, 40 mM HEPES pH 6.8, and 10 mM pyruvate). Uptake of [2-^{14}C]-radiolabeled pyruvate into mitochondria was measured by scintillation. Specific MPC activity was calculated by subtracting measurements from untreated mitochondria from those of CHC-pretreated mitochondria.

High-resolution respiratory assay. High-resolution assays of respiration were performed using an XF96 Extracellular Flux analyzer (Agilent), as described previously (36). Cells (10,000) were plated in culture media 24 hours before the assay. Before measuring respiration, culture media were replaced with DMEM, no glucose (Sigma-Aldrich D5030) supplemented with 10 mM or 1 mM pyruvate for the measurement

of pyruvate-driven respiration. For glutamine-driven respiration, culture media were replaced with glucose-free DMEM and supplemented with 10 mM glutamine. After basal respiration was measured, 0.1 μM, 0.33 μM, or 1 μM FCCP (Cayman Chemical catalog 15218) was used to stimulate uncoupled respiration. UK5099 (5 μM, Fisher catalog 418610) was administered to inhibit MPC activity; and 1 μm rotenone (Sigma-Aldrich catalog R8875) was used to inhibit complex I activity.

Coimmunoprecipitation. Crude mitochondria were resuspended in lysis buffer (20 mM Tris-Cl pH 7.4, 0.1 mM EDTA, 50 mM NaCl, 10% glycerol, 1 mM PMSF, and 1% digitonin) and incubated on ice for 30 minutes. The mitochondrial suspension was cleared by centrifugation at 8,000 *g* for 10 minutes and the supernatant collected. Supernatant was incubated with agarose beads conjugated with anti-FLAG (Sigma catalog F2426) or anti-HA (Sigma-Aldrich catalog E6779) antibody overnight at 4°C. The mixtures were loaded onto a spin column (Sigma-Aldrich catalog S3045), washed twice with lysis buffer, and eluted by incubating samples in 2× Laemmli buffer at 95°C for 10 minutes. Samples were collected by centrifugation at 8,000 *g* for 10 minutes and immunoblotted as described above.

Flow cytometry. MPC1 WT P2A GFP, M1V MPC1 WT P2A GFP, L79H P2A GFP, M1V L79H P2A GFP, R97W P2A GFP, and M1V R97W P2A GFP cDNAs were subcloned into the PQCXIB vector using NotI and EcoRV sites. These vectors were transfected into HEK 293T and 24 hours later were collected for flow cytometry analysis. Briefly, cells were washed twice with PBS and dissociated with 0.05% trypsin/EDTA (Thermo Fisher Scientific) for 5 minutes at 37°C. Trypsin was neutralized with growth media prior to centrifugation at 500 *g* for 5 minutes to pellet. Pelleted cells were resuspended with FACS buffer (PBS supplemented with 1% FBS) and analyzed by a Becton Dickinson LSR II (BD Bioscience) for GFP.

Protease inhibitor treatments. HSFs were plated at 0.5×10^6 cells per well in 6-well plates. To inhibit the ubiquitin proteasome pathway, cells were treated with 50 μM MG132 (Sigma-Aldrich catalog M7449) or vehicle for 16 hours. To inhibit autophagy, cells were treated with 100 nM bafilomycin A1 (Sigma-Aldrich catalog 19-148) or vehicle for 16 hours. Lysates were then prepared and immunoblotted as described above.

Statistics. Data are expressed as mean ± SEM. Analysis was performed by 1-way ANOVA with Holm-Sidak multiple comparison versus control post hoc test versus control or 2-tailed Student's *t* tests. Statistical outliers were identified using Grubbs' test. *P* values less than 0.05 were considered significant and differentially marked as indicated in the figure legends.

Study approval. This study utilized previously described human patient skin fibroblasts (7, 8). The Department of Clinical Research and Development Public Assistance Hospitals of Paris, in connection with the Ministry of Higher Education and Research located in Paris, France, approved skin fibroblast harvest, research use, and conservation in a research biorepository maintained in Bicêtre Hospital, Paris, France, under declaration DC 2009-939. All subjects provided informed consent prior to skin fibroblast donation and research interactions with physicians. No animals were utilized in this study.

Author contributions

LO, AJR, and EBT wrote and edited the manuscript. All authors read and commented on a draft manuscript. LO, AJR, LRG, and EBT designed or performed experiments. ACB provided updated patient information and expertise on clinical genetics.

Acknowledgments

This work was supported by NIH grants R01 DK104998 and R00 AR059190 (to EBT); T32 HL007638 to Michael Welsh (to AJR); ADA 1-18-PDF-060 (to AJR); F32 DK101183 (to LRG); and P30CA086862 to George Weiner, which contributed to support of core facilities utilized for this research. We thank Vassili Valayannopoulos, Pascal de Lonlay, and Helena Tevissen for providing the initial patient information. We thank Diana Colgan, Maria Noterman, and Diego Scerbo for providing helpful feedback on a draft manuscript. We also thank members of Taylor lab for meaningful discussions.

Address correspondence to: Eric B. Taylor, Carver College of Medicine, University of Iowa, 169 Newton Rd, PBDB 3316, Iowa City, Iowa 52204, USA. Phone: 319.384.4098; Email: eric-taylor@uiowa.edu.

1. Fantin VR, St-Pierre J, Leder P. Attenuation of LDH-A expression uncovers a link between glycolysis, mitochondrial physiology, and tumor maintenance. *Cancer Cell*. 2006;9(6):425–434.
2. Shi M, et al. A novel KLF4/LDHA signaling pathway regulates aerobic glycolysis in and progression of pancreatic cancer. *Clin*

Cancer Res. 2014;20(16):4370–4380.
3. Felig P. The glucose-alanine cycle. *Metab Clin Exp*. 1973;22(2):179–207.
4. Patel MS, Korotchkina LG. Regulation of the pyruvate dehydrogenase complex. *Biochem Soc Trans*. 2006;34(pt 2):217–222.
5. Jitrapakdee S, St Maurice M, Rayment I, Cleland WW, Wallace JC, Attwood PV. Structure, mechanism and regulation of pyruvate carboxylase. *Biochem J*. 2008;413(3):369–387.
6. Gray LR, Tompkins SC, Taylor EB. Regulation of pyruvate metabolism and human disease. *Cell Mol Life Sci*. 2014;71(14):2577–2604.
7. Bricker DK, et al. A mitochondrial pyruvate carrier required for pyruvate uptake in yeast, Drosophila, and humans. *Science*. 2012;337(6090):96–100.
8. Brivet M, et al. Impaired mitochondrial pyruvate importation in a patient and a fetus at risk. *Mol Genet Metab*. 2003;78(3):186–192.
9. Herzig S, et al. Identification and functional expression of the mitochondrial pyruvate carrier. *Science*. 2012;337(6090):93–96.
10. Tavoulari S, Thangaratnarajah C, Mavridou V, Harbour ME, Martinou JC, Kunji ER. The yeast mitochondrial pyruvate carrier is a hetero-dimer in its functional state. *EMBO J*. 2019;38(10):e100785.
11. Gray LR, et al. Hepatic mitochondrial pyruvate carrier 1 is required for efficient regulation of gluconeogenesis and whole-body glucose homeostasis. *Cell Metab*. 2015;22(4):669–681.
12. McCommis KS, et al. Loss of mitochondrial pyruvate carrier 2 in the liver leads to defects in gluconeogenesis and compensation via pyruvate-alanine cycling. *Cell Metab*. 2015;22(4):682–694.
13. Vigueira PA, et al. The beneficial metabolic effects of insulin sensitizers are not attenuated by mitochondrial pyruvate carrier 2 hypomorphism. *Exp Physiol*. 2017;102(8):985–999.
14. Rauckhorst AJ, et al. The mitochondrial pyruvate carrier mediates high fat diet-induced increases in hepatic TCA cycle capacity. *Mol Metab*. 2017;6(11):1468–1479.
15. Schell JC, et al. A role for the mitochondrial pyruvate carrier as a repressor of the Warburg effect and colon cancer cell growth. *Mol Cell*. 2014;56(3):400–413.
16. Zhong Y, et al. Application of mitochondrial pyruvate carrier blocker UK5099 creates metabolic reprogram and greater stem-like properties in LnCap prostate cancer cells in vitro. *Oncotarget*. 2015;6(35):37758–37769.
17. Wang L, et al. MPC1, a key gene in cancer metabolism, is regulated by COUPTFII in human prostate cancer. *Oncotarget*. 2016;7(12):14673–14683.
18. Zhou X, et al. Overexpression of MPC1 inhibits the proliferation, migration, invasion, and stem cell-like properties of gastric cancer cells. *Onco Targets Ther*. 2017;10:5151–5163.
19. Rauckhorst AJ, Taylor EB. Mitochondrial pyruvate carrier function and cancer metabolism. *Curr Opin Genet Dev*. 2016;38:102–109.
20. Bowman CE, Zhao L, Hartung T, Wolfgang MJ. Requirement for the mitochondrial pyruvate carrier in mammalian development revealed by a hypomorphic allelic series. *Mol Cell Biol*. 2016;36(15):2089–2104.
21. Vigueira PA, et al. Mitochondrial pyruvate carrier 2 hypomorphism in mice leads to defects in glucose-stimulated insulin secretion. *Cell Rep*. 2014;7(6):2042–2053.
22. Yang C, et al. Glutamine oxidation maintains the TCA cycle and cell survival during impaired mitochondrial pyruvate transport. *Mol Cell*. 2014;56(3):414–424.
23. Vacanti NM, et al. Regulation of substrate utilization by the mitochondrial pyruvate carrier. *Mol Cell*. 2014;56(3):425–435.
24. Gray LR, Rauckhorst AJ, Taylor EB. A method for multiplexed measurement of mitochondrial pyruvate carrier activity. *J Biol Chem*. 2016;291(14):7409–7417.
25. Timper K, et al. Mild impairment of mitochondrial OXPHOS promotes fatty acid utilization in POMC neurons and improves glucose homeostasis in obesity. *Cell Rep*. 2018;25(2):383–397.e10.
26. Schell JC, et al. Control of intestinal stem cell function and proliferation by mitochondrial pyruvate metabolism. *Nat Cell Biol*. 2017;19(9):1027–1036.
27. Grenell A, et al. Loss of MPC1 reprograms retinal metabolism to impair visual function. *Proc Natl Acad Sci U S A*. 2019;116(9):3530–3535.
28. Bender T, Pena G, Martinou JC. Regulation of mitochondrial pyruvate uptake by alternative pyruvate carrier complexes. *EMBO J*. 2015;34(7):911–924.
29. Vanderperre B, et al. MPC1-like is a placental mammal-specific mitochondrial pyruvate carrier subunit expressed in postmeiotic male germ cells. *J Biol Chem*. 2016;291(32):16448–16461.
30. Phelix CF, Bourdon AK, Dugan J, Villareal G, Perry G. MSDC-0160 and MSDC-0602 binding with human mitochondrial pyruvate carrier (MPC) 1 and 2 heterodimer: PPARγ activating and sparing TZDs as therapeutics. *IJKDB*. 2017;7(2):43–67.
31. Vanderperre B, et al. Embryonic lethality of mitochondrial pyruvate carrier 1 deficient mouse can be rescued by a ketogenic diet. *PLoS Genet*. 2016;12(5):e1006056.
32. McCommis KS, et al. Targeting the mitochondrial pyruvate carrier attenuates fibrosis in a mouse model of nonalcoholic steatohepatitis. *Hepatology*. 2017;65(5):1543–1556.
33. Shalem O, et al. Genome-scale CRISPR-Cas9 knockout screening in human cells. *Science*. 2014;343(6166):84–87.
34. Bozidis P, Williamson CD, Colberg-Poley AM. Isolation of endoplasmic reticulum, mitochondria, and mitochondria-associated membrane fractions from transfected cells and from human cytomegalovirus-infected primary fibroblasts. *Curr Protoc Cell Biol*. 2007;Chapter 3:Unit 3.27.
35. Bradford MM. A rapid and sensitive method for the quantitation of microgram quantities of protein utilizing the principle of protein-dye binding. *Anal Biochem*. 1976;72:248–254.
36. Nicholls DG, Darley-Usmar VM, Wu M, Jensen PB, Rogers GW, Ferrick DA. Bioenergetic profile experiment using C2C12 myoblast cells. *J Vis Exp*. 2010;(46):2511.